



Contents lists available at ScienceDirect

Journal of Industrial and Engineering Chemistry

journal homepage: www.elsevier.com/locate/jiec



Enhanced thermo-optical performance and high BET surface area of graphene@PVC nanocomposite fibers prepared by simple facile deposition technique: N₂ adsorption study

Mudassir Hasan^a, Arghya Narayan Banerjee^b, Moonyong Lee^{a,*}

^aSchool of Chemical Engineering, Yeungnam University, Gyeongsan 712-749, Republic of Korea

^bSchool of Mechanical Engineering, Yeungnam University, Gyeongsan 712-749, Republic of Korea

ARTICLE INFO

Article history:

Received 17 March 2014
Received in revised form 3 April 2014
Accepted 7 April 2014
Available online xxx

Keywords:

PVC
Graphene
Nanocomposite
Fibers
Surface area
Thermal stability
Glass transition temperature
Activation energy

ABSTRACT

GN@PVC nanocomposite fiber was synthesized by simple facile deposition technique using THF as a solvent. The as-prepared GN@PVC nanocomposite fibers were characterized by BET, Raman, XPS, XRD, TEM, TGA, DRS and SEM. BET analysis of GN@PVC showed 70% enhancement in the surface area over PVC fibers. The thermal stability of GN@PVC nanocomposite fibers was found to be highly dependent on the weight percent of GN and nanocomposite with 3 wt.% GN showed 8% increase in glass transition temperature and 36% improvement in the activation energy for thermal degradation. Moreover, GN@PVC nanocomposite fibers showed lower band gap in comparison to PVC.

© 2014 The Korean Society of Industrial and Engineering Chemistry. Published by Elsevier B.V. All rights reserved.

1. Introduction

Recently organic–inorganic composites have attracted considerable attention of researchers worldwide due to their possible applications in various fields such as electronics [1], chemistry [2], biology [3], and medicine [4]. On the other hand, substantial enhancement of the mechanical, thermal, optical and barrier properties can be obtained using nanofillers. Compared to traditional micro-fillers, excellent properties can be obtained with very low nanofiller loading without substantially increasing the density and cost or reducing the light transmission properties of the base polymer. Therefore systematic study of the properties of these polymer nanocomposites will help in finding more applications for practical use.

Graphene (GN), a planar two-dimensional form of carbon, is one of the most exciting materials today because of its unique properties [5]. Individual GN sheets have a large surface area [6], high thermal conductivity [7], high Young's modulus [8], ballistic transport on the sub-micron scale, and mass-less Dirac

fermion charge carrier ability [9]. The outstanding properties of GN has made it a promising material for many applications, such as photovoltaic devices, transparent electrodes, sensors, super capacitors, and conducting composites [10–15].

Polyvinyl chloride (PVC) is one of the most versatile and widely used polymer. Moreover, it is a low cost, chemically stable, biocompatible and sterilizable polymer [16]. The problem associated with PVC is its low thermal stability, which hinders some of its applications [17]. Therefore, enhancing thermal stability along with high mechanical strength and electrical conductivity of PVC by using nanofillers is highly desirable from an application point of view. Many carbon-based materials have been used as fillers in the past decade to achieve this goal, such as clay [18], wood fibers [19] and calcium carbonate [20], and have been used to improve the thermal and mechanical performance of PVC. Carbon nanotubes (CNTs) have also been used as fillers to improve the electrical and thermal conductivities [21]. Sajini et al. [22] reported that GN-filled PVC nanocomposite films showed flexible conductivity, high mechanical strength and thermal stability.

PVC fibers can be produced using many different techniques, such as melt-spinning, wet-spinning and dry-spinning. On the other hand, these methods not only require some chemicals or

* Corresponding author. Tel.: +82 53 810 2512.
E-mail address: mynlee@ynu.ac.kr (M. Lee).

elevated temperatures, but are also expensive. Moreover, the fibers produced using these techniques are inherently less thermally stable. Therefore, the aim of the present work was to prepare PVC fibers with GN as a nanofiller to impart high thermal stability and greater surface area to the fiber. To the best of the authors' knowledge, there are few reports on the synthesis and characterization of GN-based PVC nanocomposite fibers. Therefore, this work is expected to be useful to the scientific community working in the field of composite materials for practical applications. In this study, GN@PVC nanocomposite fibers were prepared using a simple and facile deposition technique. The structure, morphology, thermal stability, optical, and adsorption properties were also examined.

2. Experimental

2.1. Materials

PVC (average molecular weight ~ 1020) was purchased from Yakuri Pure Chemicals, Japan and GN was obtained from Iljin Nano Tech, Seoul, Korea (thickness ~ 8 nm and mean length ~ 500 nm). Tetrahydrofuran (THF) was supplied by Duksan Pure Chemicals, Korea, and was used as received.

2.2. Preparation of the GN@PVC nanocomposite fibers

The GN@PVC fibers were prepared in two steps: firstly the synthesis of GN@PVC nanocomposites by mixing GN in the THF solution of PVC followed by the deposition technique to prepare the GN@PVC fibers. In a typical process, PVC was first dissolved in 50 mL of THF with continuous stirring for 24 h for complete dissolution. GN was mixed with the above solution under continuous stirring and occasional shaking in bath ultrasonic system for 5 min to allow proper dispersion of GN inside the THF solution of PVC. Subsequently, the mixture was poured in distilled water with vigorous stirring to obtain the GN@PVC fibers. The fibers were washed with distilled water and excess of methanol, later dried at 60°C in an air oven for 24 h. Pure PVC fibers were also prepared using a similar route in the absence of GN. Table S1 lists the preparation conditions.

2.3. Characterization

Structural analyses of the samples were carried out by X-ray diffraction (XRD, PAN analytical, X'pert PRO-MPD) in the range, $10\text{--}90^\circ 2\theta$, using Cu $K\alpha$ radiation ($\lambda = 0.15405$ nm). Raman spectroscopy (InVia Reflex UV Raman microscope, Renishaw, UK) was used to study the type of interaction between PVC and GN in nanocomposite fibers. X-ray energy photoelectron spectroscopy

(XPS, ESCALAB 250) was performed using a monochromatized Al $K\alpha$ X-ray source ($h\nu = 1486.6$ eV) with a $500\ \mu\text{m}$ spot size. The surface morphology was examined by scanning electron microscopy (SEM, Hitachi-4200). The optical properties were determined by ultraviolet-visible-near infrared (UV-VIS-NIR, VARIAN, Cary 5000, USA) spectrophotometry. The microstructural properties were analyzed by field emission transmission electron microscopy (FE-TEM, TecnaiG2 F20, FEI, USA) operating at an accelerating voltage of 200 kV. Thermogravimetric analysis (TGA, SDT Q600, USA) was performed by heating the samples from 25°C to 800°C at a rate of $10^\circ\text{C min}^{-1}$ in a nitrogen atmosphere. Differential scanning calorimetry (DSC, Q 200, USA) was performed by heating the samples from 20°C to 120°C . The Fourier transform infrared (FTIR) spectra were recorded using a Nicolet 6700 FTIR spectrometer. The nitrogen adsorption isotherm of our PVC and GN@PVC fibers at 77 K was obtained by using a Quantachrome, Asic-7 physisorption analyzer. In the analysis, the fibers were degassed at 250°C in vacuum for 1 h before the nitrogen adsorption isotherm was constructed. The surface area of fibers was evaluated by the Brunauer–Emmett–Teller (BET) model, while the pore size and pore volume were estimated with Barrett–Joyner–Halenda (BJH) theory.

3. Result and discussion

3.1. Preparation of PVC, GN@PVC nanocomposite fibers

A simple facile deposition technique was used for the preparation of GN@PVC nanocomposite fibers using two immiscible solvent systems, i.e. THF and water. The dispersed GN@PVC in THF solvents under vigorous stirring readily got precipitated in water due to its insolubility in water. The fibers were a few micrometers in thickness and several micrometers in length (Fig. 1). The surface area of the fibers is expected to increase after incorporating GN into the PVC matrix due to high surface area of nanomaterials, which is desirable for the surface-related properties, such as adsorption and catalysis.

3.2. X-ray diffraction (XRD)

Fig. 2 shows XRD patterns of the GN@PVC nanocomposite fibers and GN. In the case of PVC (Fig. S1), the peak at $13^\circ 2\theta$, clearly shows its poor crystallinity owing to the high integrated area. In addition, more amorphous peaks at 16.5° and $24.5^\circ 2\theta$ were also observed. These observations confirmed that PVC is a multiphase, possessing both poor crystalline and highly amorphous regions.

The XRD patterns of the pure GN nanoparticles (Fig. 2, inset) clearly showed a sharp peak at $26.5^\circ 2\theta$, which was very close to

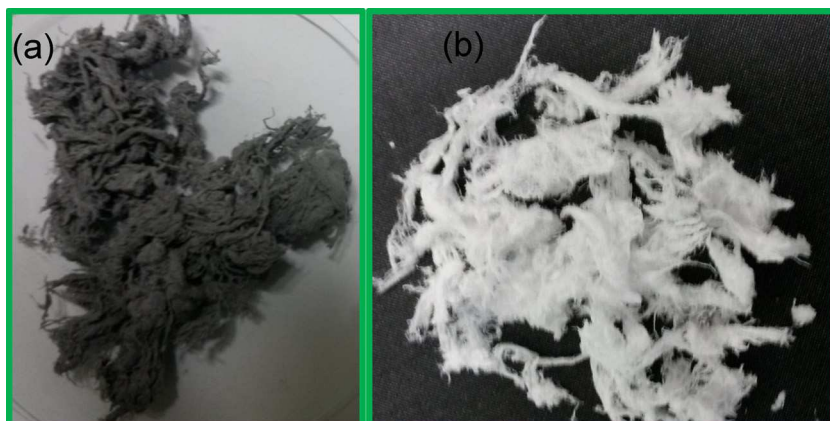


Fig. 1. Digital photograph of (a) GN@PVC-3% nanocomposite fibers and (b) PVC fibers.

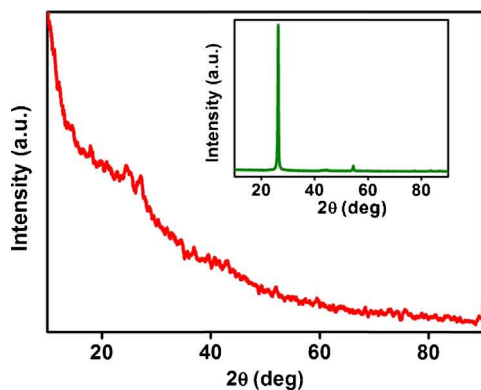


Fig. 2. XRD patterns of the GN@PVC-3% nanocomposite fibers (pure GN is in the inset).

the typical diffraction peak of graphite corresponding to the spacing between single GN layers ($d = 0.33$ nm). Smaller peaks were also observed at a higher angle (44° , 55° , 77° and 84° 2θ). The XRD patterns of the GN@PVC-1% nanocomposite fibers (Fig. S2) revealed the broadening of peak of GN (26.5° 2θ), which might be due to presence of PVC fibers. However, with the higher loading of GN, little more pronounced peaks of GN can be seen (Fig. 2). The decrease in the crystallinity of GN in GN@PVC nanocomposites can be interpreted on the basis that PVC is highly amorphous and has a significant effect on the crystallinity of GN in terms of beige formation resulting in decrease in peak intensity.

3.3. Raman spectroscopy

Raman spectroscopy is a powerful tool for characterizing the effect of interactions on the molecular structure of a component present in a nanocomposite system. The Raman spectra of the GN@PVC-3% nanocomposite fibers showed two characteristic bands, the D band and G band (Fig. 3). The D band was attributed to a disordered graphite structure, whereas the G band showed the structural intensity of the sp^2 -hybridized carbon atoms. The presence of both bands in the Raman spectra of the GN@PVC-3% nanocomposite fibers suggests that the nanocomposite contains both sp^3 and sp^2 -hybridized carbon atoms in good proportions. The difference in the band intensity ratio (I_D/I_G) of the GN and nanocomposite can be used to estimate the relative degree of defects in the GN. The value of intensity ratio between the D and G bands (I_D/I_G) was calculated to be 1.07 and 0.29 for GN@PVC-3% nanocomposite fibers and pure GN, respectively. If both bands have similar intensity, that is if $I_D/I_G \approx 1$, it indicates a high quantity of structural defects. The increase in the I_D/I_G ratio of nanocomposite

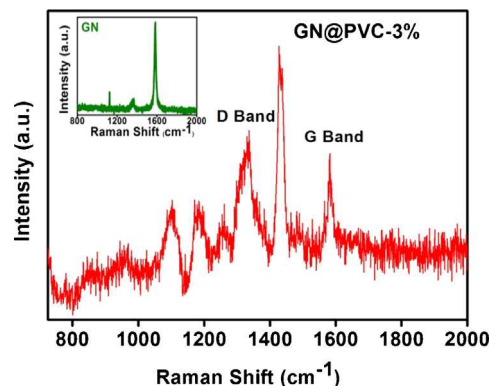


Fig. 3. Raman spectra of the GN@PVC-3% nanocomposite fibers (pure GN is in the inset).

fibers obtained in our case in comparison to GN indicates an increase in the defects in the lattice of GN [21]. The positions of the D and G bands were also affected, confirming that defect was formed in the GN structure after the addition of GN into the PVC matrix. On account of the various defects induced it can be concluded that the property of GN@PVC-3% nanocomposite fiber is altered and GN@PVC nanocomposite fibers will probably show different properties than PVC fibers.

3.4. Scanning electron microscopy

Fig. 4 shows SEM images of PVC and GN@PVC-3% nanocomposite fibers. Long strands of PVC and GN@PVC-3% nanocomposite fibers with loose cotton like morphology can be clearly seen from the figure. The loose cotton like structures greatly enhances the surface area of PVC and GN@PVC-3% nanocomposite fibers, indicating the suitability of the method for the preparation of fibrous structures.

3.5. Transmission electron microscopy (TEM)

Fig. 5 shows TEM images of the GN@PVC-3% nanocomposite fiber. The low-magnification TEM images (Fig. 5) clearly depict the GN@PVC-3% nanocomposite fibers attached to the GN sheet. In addition, TEM showed that GN is thin, and layered, as well as well dispersed within the GN@PVC-3% nanocomposite fibers. The mean thickness and length of the GN@PVC nanocomposite fibers was measured to be 2.75 and 8 μm , respectively (Fig. 5). The TEM images of the nanocomposite fibers clearly showed the successful incorporation of GN inside PVC, which may give rise to enhanced thermal stability (Fig. 6) and increased surface area.

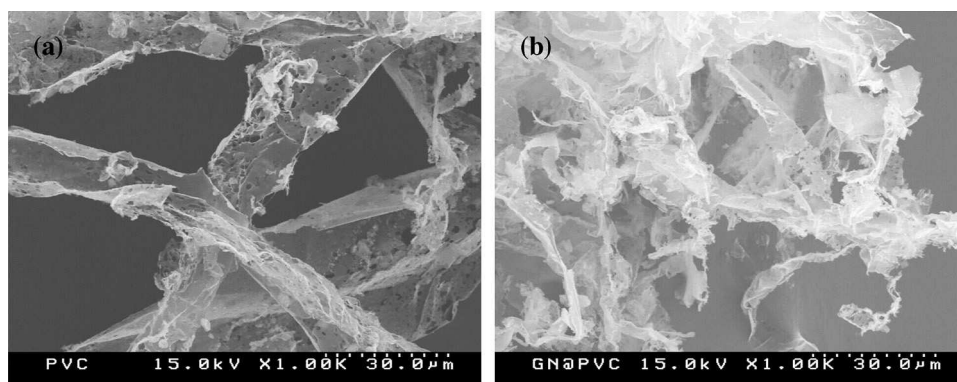


Fig. 4. SEM images of (a) PVC and (b) GN@PVC fibers.

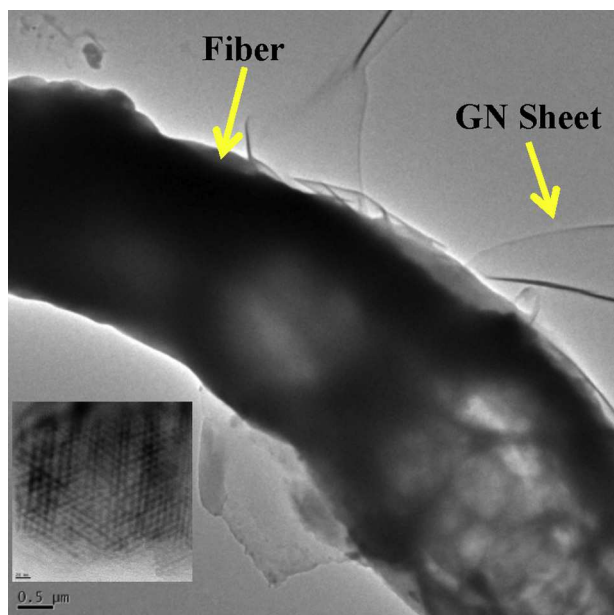


Fig. 5. TEM images of GN@PVC nanocomposite fiber and HRTEM image of GN (in the inset).

3.6. Thermogravimetric analysis

TGA is an analytical technique used to determine the thermal stability of a material. The fraction of the volatile components present in the material can also be determined by monitoring the weight change that occurs as the sample is heated [23]. Fig. 6 shows the TGA curves of the PVC and GN@PVC nanocomposite fibers. The weight loss below 100 °C for both PVC and GN@PVC-3% nanocomposite fibers can be attributed to the evaporation of trapped THF and other volatile components. Both PVC and nanocomposite fibers showed a two-stage degradation process. Two major weight losses occurred in all cases (Fig. 6). In the case of PVC, the first weight loss was observed in the range, 260–360 °C, which corresponds to the loss of HCl [24]. At this temperature, the Cl radicals formed from the cleavage of –C–Cl bonds abstract hydrogen from the neighboring C–H bonds, resulting in the evolution of HCl molecules from the polymer chain. Once the reaction is initiated, “allyl” activation continues and the Cl atoms become dislocated along the macromolecule chain, leaving behind a polyene backbone [24]. The second major weight loss was observed in the range, 421–500 °C, which was much shorter than the first stage. Thermal degradation of the polyene backbone takes

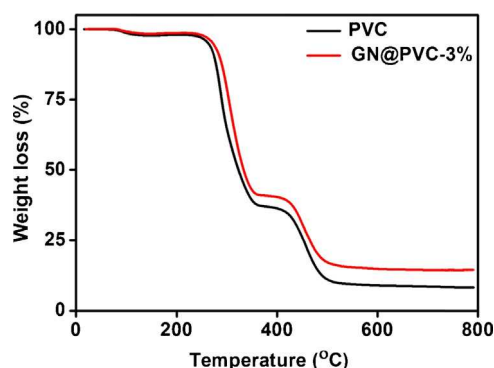


Fig. 6. TGA data of the PVC and GN@PVC nanocomposite fiber.

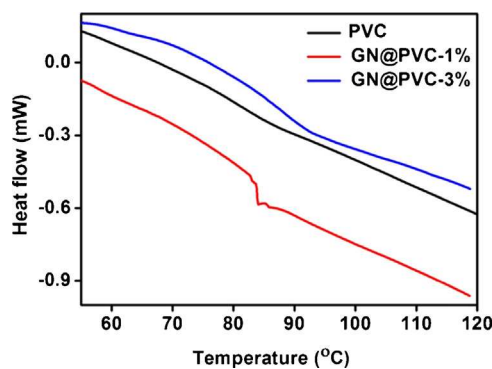


Fig. 7. DSC thermograms of pure PVC and GN@PVC nanocomposite fibers.

place at this stage, resulting in the formation of volatile aromatic compounds and a stable carbonaceous residue [25].

On the other hand, the TGA curve of the GN@PVC-3% nanocomposite fibers (Fig. 6) showed a shift in the thermal degradation onset temperature for the first and second major weight loss from 260 °C to 266 °C and 421 °C to 427 °C, respectively, suggesting the increased thermal stability of the nanocomposite fibers after the incorporation of GN. A possible reason for the enhanced stability is the higher thermal stability of GN and there might also be some sort of stabilizing interaction between the GN and PVC. Similar reports with increased thermal stability after the incorporation of GN also been reported by Omaish et al. [7] in their nanocomposite of polyaniline with GN.

3.7. Differential scanning calorimetry

Fig. 7 shows the DSC thermograms of the PVC and GN@PVC nanocomposite fibers with different loadings of GN. The thermograms of the heat flow rate versus temperature showed a distinct hump relaxation at around 77–94 °C for all GN@PVC nanocomposite fibers, which is the glass transition temperature (T_g) of the nanocomposite fibers. Fig. 8 shows T_g of the nanocomposite fibers with different weight contents of GN. T_g of the nanocomposite fibers were found to be 80, 83.78 and 86.49 °C for PVC, GN@PVC-1% and GN@PVC-3% respectively. Thus it can be seen that GN has significant effect on the glass transition temperature of GN@PVC nanocomposite fibers. The glass transition temperature of PVC was observed to be around 80 °C and with increase in GN loading, the nanocomposites showed significant enhancement in the glass transition temperature. The T_g increases with the percentage of GN, which can be interpreted as the reinforcing effect of GN which reduces the chain segmental mobility, hence, an enhancement in T_g [22].

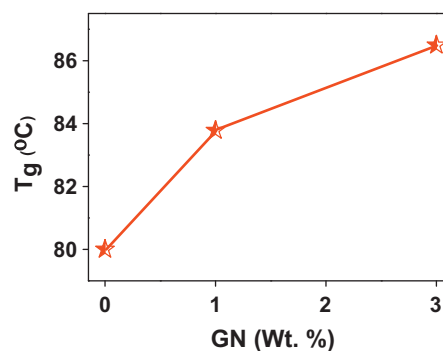


Fig. 8. Glass transition temperature (T_g) of the GN@PVC nanocomposite fibers at various weight fractions of GN in the PVC matrix.

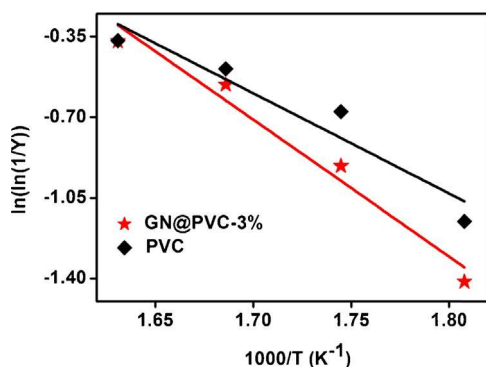


Fig. 9. Plot of $\ln(\ln(1/Y))$ vs. $1000/T$ (K^{-1}) to estimate the activation energy for the thermal degradation of PVC and GN@PVC nanocomposite fibers.

The activation energy (E_a) for the thermal degradation of the GN@PVC-3% nanocomposite fibers and PVC was evaluated using the well-known integral method reported by Broido [26,27].

$$\ln\left(\ln\left(\frac{1}{Y}\right)\right) = \frac{-E_a}{RT} + C \quad (1)$$

$$Y = \frac{W_T - W_\infty}{W_0 - W_\infty} \quad (2)$$

where Y is the fraction of the samples not yet decomposed, W_0 and W_∞ are the initial and final weights, respectively, and W_T is the weight at the particular temperature. The plots of $\ln(\ln(1/Y))$ versus $1000/T$ (K^{-1}) (as shown in Fig. 9) followed a straight line, whose slope gave the activation energy for the thermal degradation process. The activation energies of PVC and GN@PVC-3% nanocomposite fibers were estimated to be 36 and 49 kJ/mol, respectively. The Arrhenius factor for thermal degradation of PVC and GN@PVC-3% nanocomposite fibers was calculated from the intercept of the plots of $\ln(\ln(1/Y))$ versus $1000/T$ (K^{-1}) and was obtained to be 6.8 and 9.4 for PVC and GN@PVC-3% respectively. Therefore, the higher activation energy for degradation of GN@PVC-3% nanocomposite fibers in comparison to PVC further supports the higher stability of GN@PVC-3% nanocomposite fibers which also corresponds with the TGA results (Fig. 6).

3.8. FT-IR analysis

Fig. 10 shows the FT-IR spectra of the PVC and GN@PVC-3% nanocomposite fibers. In the case of PVC, absorption bands were observed at 611, 964, 1251, 1631 and 2913 cm^{-1} . Table S2 lists the characteristic absorption bands of pure PVC. The FT-IR

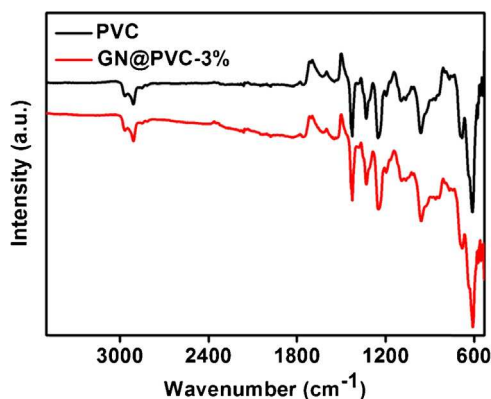


Fig. 10. FT-IR spectra of PVC and GN@PVC nanocomposite fibers.

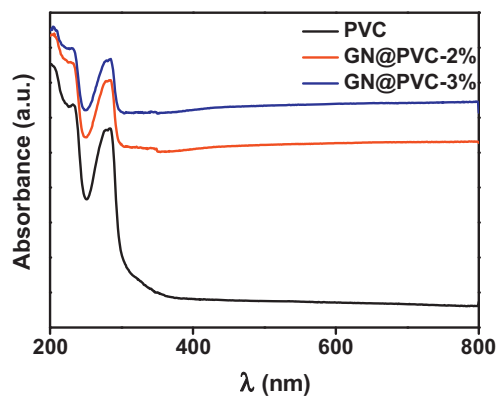


Fig. 11. UV-visible diffuse absorbance spectra of PVC and GN@PVC nanocomposite fibers.

spectrum of the GN@PVC-3% nanocomposite was found to be similar to that of PVC. The GN@PVC-3% nanocomposite fibers showed no shift in the bands compared to the pure PVC spectrum, suggesting little or no interactions between the GN nanoparticles and pure PVC in terms of chemical bonding.

3.9. Optical property analysis

Both the GN@PVC nanocomposite fibers and PVC showed strong absorption in the UV region (Fig. 11). The nanocomposite fibers showed enhancement in absorption compared to PVC and with the GN loading of 2 and 3 wt. % in PVC, the absorbance of the nanocomposite fibers increased by 23 and 33%, respectively. The absorbance spectra showed three absorbance peaks at $\lambda = 207$, 231, and 281 nm, which were assigned to the $n-\sigma^*$, $n-\pi^*$, and $\pi-\pi^*$ transition, respectively.

To determine the band gap of the PVC and GN@PVC nanocomposite fibers, the approximate relationships among the reflectance (R) (Fig. 12), absorption coefficient (α), and scattering coefficient (s) based on Kubelka–Munk theory was adopted, assuming no transmission within the nanomaterials as the fibers formed in our case are thin fibers in micron range [28].

$$\alpha = \frac{s}{2((1 - R)^2/R)} \quad (3)$$

In Eq. (3), both α and s are functions of the energy of incident radiation ($h\nu$). On the other hand, s is far less wavelength dependent than α in the region of strong absorption. Hence, s was assumed to be constant at the onset of the absorption edge. The band gap of the GN@PVC nanocomposite fibers was determined

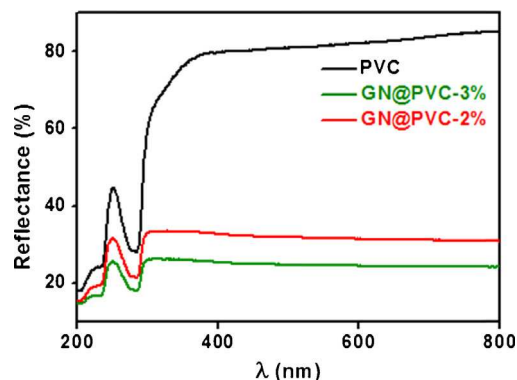


Fig. 12. UV-visible diffuse reflectance spectra of PVC and GN@PVC nanocomposite fibers.

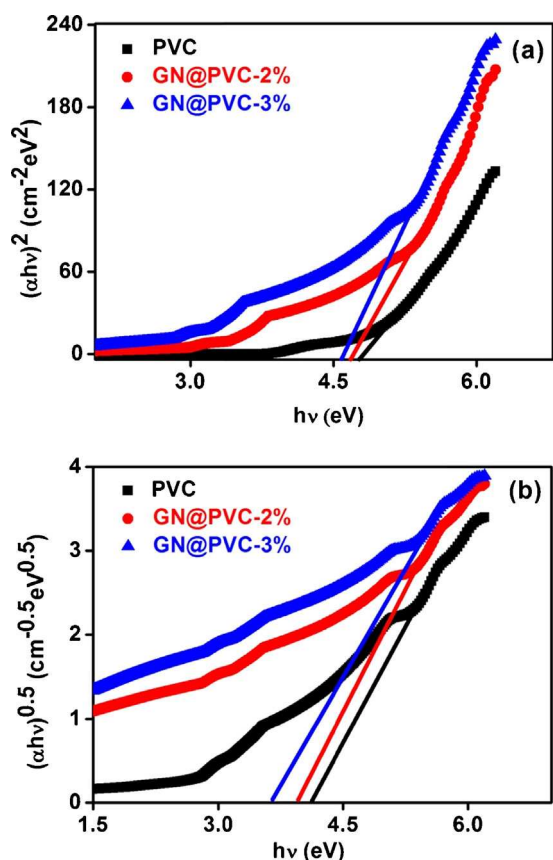


Fig. 13. (a) Direct band gap calculation for PVC and GN@PVC nanocomposite fibers and (b) Indirect band gap calculation for PVC and GN@PVC nanocomposite fibers.

from the absorption coefficient (α) using the following equation [29]:

$$(\alpha hv)^{1/x} = A(hv - E_g) \quad (4)$$

This equation was formulated by the relationship for the parabolic bands at the onset of the absorption edge, where $h\nu$ is the incident photon energy, A is a material constant, and x is an exponent that depends on the type of transition. In a direct band gap the electron only needs energy to jump to the conduction band while in an indirect band electron needs energy and momentum to jump to the conduction band. Indirect band gap can be defined on the basis that the minimum energy in the conduction band and the maximum energy in the valence band occur at different values of the crystal momentum, indicating that a direct transition from the valence (V.B.) to the conduction band (C.B.) of an electron requires a photon of energy higher than that of the direct band gap. The value of x in the case of a direct allowed transition, indirect allowed transition and direct forbidden transition is $1/2$, 2 and $3/2$, respectively. The band gap was determined by a plot of $(\alpha hv)^{1/x}$ and $h\nu$ at approximately the fundamental absorption region (Fig. 13a and b).

Fig. 13a and b shows the direct and indirect band gap calculation for the PVC and GN@PVC nanocomposite fibers. The direct and indirect allowed band gaps of all nanocomposite fibers

Table 1
Band gap for direct allowed and indirect allowed transitions.

Sample	Direct allowed E_g (eV)	Indirect allowed E_g (eV)
PVC	4.76	4.13
GN@PVC-2%	4.68	3.95
GN@PVC-3%	4.58	3.63

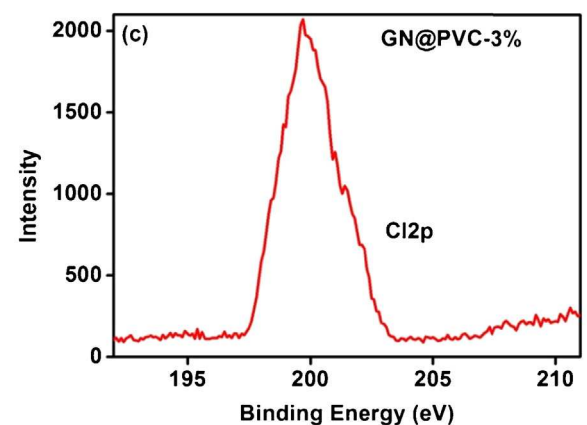
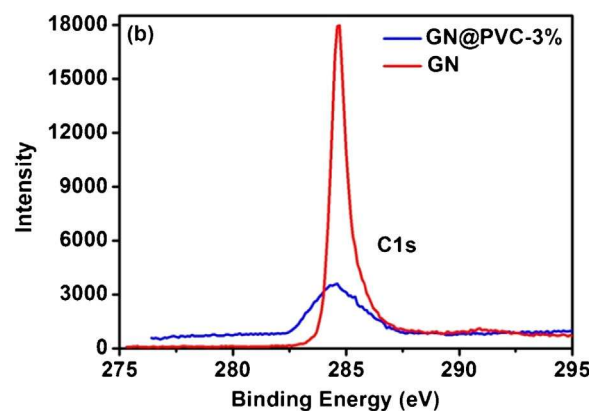
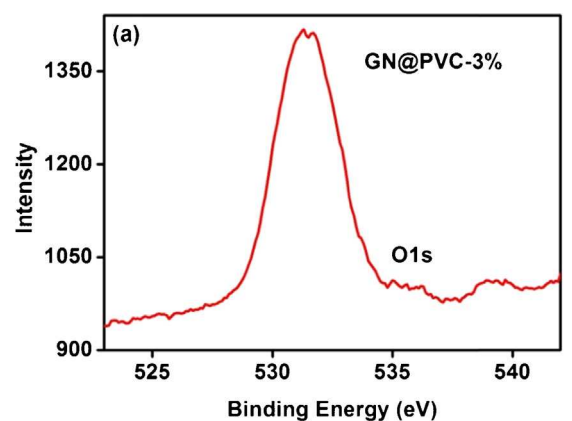


Fig. 14. XPS spectra of GN and GN@PVC-3% nanocomposite fibers for (a) O1s peak, (b) C1s peaks, and (c) Cl2p peak.

were lower than those of PVC (Table 1). The obtained direct and indirect band gaps of PVC were 4.76 and 4.13 eV, respectively. Emad et al. [30] and Bushra et al. [31] reported similar direct and indirect band gaps for PVC thin films. The decrease in the direct and indirect band gap in our case for GN@PVC nanocomposite fibers were attributed to the formation of polarons in the fibers of the PVC loaded with GN. Some modifications in the size of the amorphous domains in PVC due to the incorporation of GN may also explain the optical band gap reduction for the nanocomposite fibers [30].

3.10. XP spectra

The surface characterization and chemical states of GN and GN@PVC nanocomposite fiber was performed by XPS. Fig. 14a presents the O1s spectra of GN@PVC-3% nanocomposite fibers, which could be attributed to the presence of residual oxygen, due

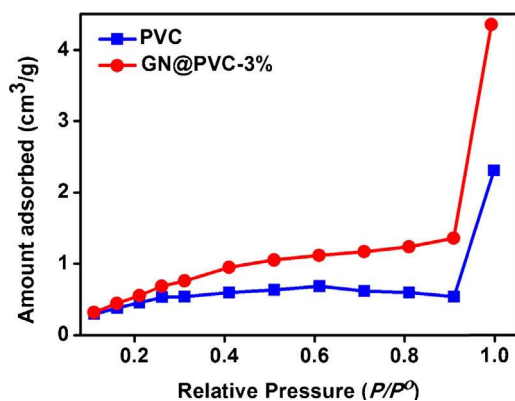


Fig. 15. N_2 adsorption isotherms of PVC and GN@PVC-3% nanocomposite fibers.

Table 2

Physical properties deduced from N_2 adsorption at 77 K on PVC and GN@PVC nanocomposite fibers.

Samples	Surface area (m^2/g)	Average pore volume (cm^3/g)	Average pore diameter (nm)
PVC	2.018	5.467×10^{-3}	26.74
GN@PVC-3%	3.439	9.422×10^{-3}	18.84

to some trapped THF during the fiber synthesis. Fig. 14b presents C1s spectra of GN and GN@PVC-3% nanocomposite fibers. The slight change in the binding energy of C1s from 284.68 to 284.45 eV in the case of GN and GN@PVC-3% nanocomposite fiber respectively is probably due to strong interaction between the carbon of GN and chlorine of PVC. Fig. 14c presents the core level Cl2p spectra of the GN@PVC-3% nanocomposite fibers. The binding energy of the Cl2p peak was found to be ~ 200 eV, which is in good agreement with the previous reported binding energy (200.8 eV) of Cl2p for PVC [32].

3.11. Adsorption isotherms

Fig. 15 shows the N_2 adsorption isotherms measure on the PVC and GN@PVC-3% nanocomposite fibers. Both the isotherms showed the presence of a hysteresis loop, which is a characteristic feature of the type IV isotherms [33]. In the case of PVC fibers, the isotherm initially showed an initial ascending section up to $p/p^\circ = 0.27$, afterwards it showed a rather straight section, which extended up to $p/p^\circ = 0.91$. Finally, the isotherm exhibited an upward sweep near saturation pressure. Similar pattern of isotherm was observed in case of GN@PVC-3% nanocomposite fibers, except that the initial ascending section extended up to $p/p^\circ = 0.41$. The enhancement in the N_2 adsorption at high p/p° values was observed greater for GN@PVC-3% nanocomposite fibers. The adsorption isotherms indicated that the pores are mesoporous. After the incorporation of GN into PVC, BET surface area and pore volume of GN@PVC-3% nanocomposite fibers greatly increased (Table 2), while the pore size decreased.

4. Conclusions

GN@PVC nanocomposite fibers were synthesized using a simple facile deposition technique and the adsorption, thermal, structural, and optical behaviors of the nanocomposite fibers were examined by

range of different techniques. GN@PVC with a 3 wt.% GN loading showed 70% enhancement in the surface area over PVC fibers. The GN@PVC nanocomposite fibers compared to the PVC fibers showed greater stability toward thermal degradation. The GN@PVC nanocomposite fibers showed a lower optical band gap than PVC due to the formation of polarons within the nanocomposite. At a 3 wt.% GN loading, T_g and E_d for the thermal degradation of the nanocomposite fiber were enhanced by 8% and 36%, respectively. Owing to its enhanced surface area and better thermo-optical properties, this nanocomposite material is expected to find suitable role for a range of practical applications, such as adsorption, photodegradation, and materials which requires combination of high surface area and thermal stability.

Acknowledgement

This study was supported by Yeungnam University Research Grant (2012).

Appendix A. Supplementary data

Supplementary data associated with this article can be found, in the online version, at doi:10.1016/j.jiec.2014.04.019.

References

- [1] C. Wang, R. Cheng, L. Liao, X. Duan, *Nanotoday* 18 (5) (2013) 514.
- [2] J. Zuo, Y. Wang, T.S. Chung, *J. Membr. Sci.* 433 (2013) 60.
- [3] K. Rezwani, Q.Z. Chen, J.J. Blaker, A.R. Boccacini, *Biomaterials* 27 (18) (2006) 3413.
- [4] A. Abdal-hay, M. Dewidar, J. Lim, J.K. Lim, *Ceram. Int.* 40 (1) (2014) 2237.
- [5] S.K. Yadav, J.W. Cho, *Appl. Surf. Sci.* 266 (2013) 360.
- [6] S.K. Yadav, H.J. Yoo, J.W. Cho, *J. Polym. Sci. B: Polym. Phys.* 51 (2013) 39.
- [7] M.O. Ansari, S.K. Yadav, J.W. Cho, F. Mohammad, *Composites B* 47 (2013) 155.
- [8] C. Lee, X.D. Wei, J.W. Kysar, J. Hone, *Science* 321 (5887) (2008) 385.
- [9] Y.B. Zhang, Y.W. Tan, H.L. Stormer, P. Kim, *Nature* 438 (7065) (2005) 201.
- [10] Z.F. Liu, Q. Liu, Y. Huang, Y.F. Ma, S.G. Yin, X.Y. Zhang, *Adv. Mater.* 20 (20) (2008) 3924.
- [11] J.T. Robinson, F.K. Perkins, E.S. Snow, Z.Q. Wei, P.E. Sheehan, *Nano Lett.* 8 (10) (2008) 3137.
- [12] P.K. Ang, W. Chen, A.T.S. Wee, K.P. Loh, *J. Am. Chem. Soc.* 130 (44) (2008) 14392.
- [13] M.O. Ansari, M.M. Khan, S.A. Ansari, I. Amal, J. Lee, M.H. Cho, *Chem. Eng. J.* 242 (2014) 155.
- [14] M.O. Ansari, M.M. Khan, S.A. Ansari, I. Amal, J. Lee, M.H. Cho, *Mater. Lett.* 114 (2014) 159.
- [15] T. Ramanathan, A.A. Abdala, S. Stankovich, D.A. Dikin, M. Herrera-Alonso, R.D. Piner, *Nat. Nanotechnol.* 3 (6) (2008) 327.
- [16] C.E. Wilkes, J.W. Summers, C.A. Daniels, M.T. Berard, *PVC Handbook*, first ed., Hanser-Verlag, Germany, 2005p. 414.
- [17] B. Ivan, T. Kelen, F. Tudos, in: H.H.G. Jellinek, H. Kachi (Eds.), *Degradation and Stabilization of Polymers*, Elsevier Science, Amsterdam, Netherlands, 1989, p. 483.
- [18] T. Peprnicek, A. Kalendova, E. Pavlova, J. Simonik, J. Duchet, J.F. Gerard, *Polym. Degrad. Stab.* 91 (12) (2006) 3322.
- [19] L.M. Matuana, C.B. Park, J.J. Balatinecz, *Polym. Eng. Sci.* 38 (11) (1998) 1862.
- [20] S.S. Sun, C.Z. Li, L. Zhang, H.L. Du, J.S. Burnell-Gray, *Polym. Int.* 55 (2) (2006) 158.
- [21] V.J. Mkhabela, A.K. Mishra, X.Y. Mbianda, *Carbon* 49 (2011) 610.
- [22] V. Sajini, P. Jinu, M. Narahari, V. Suresh, *Carbon* 49 (2011) 198.
- [23] Z. Dobkowski, *Polym. Degrad. Stab.* 91 (2006) 488.
- [24] G.W. Becker, *Kolloidn. Zh.* 140 (1) (1955) 1.
- [25] M. Kawasumi, N. Hasegawa, M. Kato, A. Usuki, A. Okada, *Macromolecules* 30 (20) (1997) 6333.
- [26] A. Rangraj, V. Vangani, K. Rakshit, *J. Appl. Polym. Sci.* 66 (1997) 45.
- [27] P.S. Abthagir, R. Saraswathi, S. Sivakolunthu, *Thermochim. Acta* 411 (2004) 109.
- [28] J.D. Lindberg, D.G. Synder, *Appl. Opt.* 12 (1973) 573.
- [29] J.I. Pankove, *Optical Process in Semiconductors*, Prentice-Hall, New Jersey, 1971.
- [30] E. Yousif, M. Abdullah, H. Hashim, N. Salih, J. Salimon, B.M. Abdullah, *Int. J. Ind. Chem.* 4 (2013) 4.
- [31] B.A. Hasan, M.A. Saeed, A.A. Hasan, *Br. J. Sci.* 7 (2012) 14.
- [32] G. Beamson, D. Briggs, *High Resolution XPS of Organic Polymers*, John Wiley, Chichester, England, 1992p. 208.
- [33] S.J. Gregg, K.S.W. Sing, *Adsorption, Surface Area and Porosity*, second ed., Academic Press, London, 1982.